Functional precision oncology for follicular lymphoma with patient-derived xenograft in avian embryos

Manon Zala, Boris Lipinski, Clélia Costechareyre, Loraine Jarrosson, Romain Teinturier, Edith Julia, Marjorie Lacourrège, Aurélie Verney, Jérôme Guitton, Alexandra Traverse-Glehen, et al.

Functional precision oncology for follicular lymphoma with patient-derived xenograft in avian embryos

Manon Zala[1], Boris Lipinski[1*], Clélia Costechareyre[2*], Loraine Jarrosson[2*], Romain Teinturier[2], Edith Julia[1], Marjorie Lacourrège[2], Aurélie Verney[1], Jérôme Guitton[3], Alexandra Traverse-Glehen[1,4], Emmanuel Bachy[1], Gilles Salles[5], Sarah Huet[1,7], Laurent Genestier[1], Valérie Castellani[6], Céline Delloye-Bourgeois[6], Pierre Sujobert[1,7]

1. Centre International de Recherche en Infectiologie (CIRI, INSERM U1111, CNRS UMR 5308), Lymphoma immunobiology team, faculté de médecine Lyon Sud, Université Lyon 1
2. OncoFactory, an ERBC company, Faculté de Médecine et de Pharmacie, 8 avenue Rockefeller 69008 Lyon, France
3. Hospices Civils de Lyon, Hôpital Lyon Sud, Service de biochimie
4. Hospices Civils de Lyon, Hôpital Lyon Sud, Service d'Anatomopathologie
5. Lymphoma Service, Department of Medicine, Memorial Sloan Kettering Cancer Center, New York, NY
6. University of Lyon, University Claude Bernard Lyon 1, MeLiS, CNRS UMR5284, INSERM U1314, NeuroMyoGene Institute, 69008 Lyon, France
7. Hospices Civils de Lyon, Hôpital Lyon Sud, Service d'hématologie biologique, Pierre Bénite, France

* contributed equally to the work

Running Title: Follicular lymphoma PDX in avian embryo.

Keywords: follicular lymphoma; RCHOP; *BAX*; functional precision oncology; avian embryo xenograft.

Additional information:
Financial support: this work was supported by grants from the Agence Nationale de la Recherche (ANR-19-CE17-005-01) and financial support from the Hospices Civils de Lyon.

Corresponding author: Pierre Sujobert, Service d'hématologie biologique, Hôpital Lyon Sud, 165 chemin du grand Revoyet. 69310 Pierre Bénite, France. pierre.sujobert@chu-lyon.fr Tel.: +33 4788615 / Fax: +33 478864104

Conflict of interest statement: CC, LJ, ML and RT are employed by Oncofactory, an ERBC company. VC and CDB are co-founders of Oncofactory SAS.

Word-abstract: 150

Word statement of significance: 24

Word of text: 3486

References: 26

4 figures, 4 supplemental figures and 6 supplemental tables.

Abstract

Despite achieving high rates of complete remission with RCHOP immuno-chemotherapy, almost all patients with follicular lymphoma (FL) will experience multiple relapses after treatment. The lack of experimental model of FL limits our understanding of treatment response heterogeneity. Here we characterized a new model of FL patient-derived xenograft in avian embryos. Based on 20 biopsy samples, we observed that tumor volume reduction achieved with RCHOP treatment *in ovo* predicted progression free survival in multivariate analysis. To further explore the model, we used single-cell RNA sequencing to discover a signature of 21 genes upregulated after RCHOP exposure, with significant intratumoral heterogeneity. Among these genes, we functionally validated *BAX* as a critical effector of RCHOP which can be targeted with venetoclax *in vitro* and *in ovo*. Overall, the FL-AVI-PDX model is a platform for functional precision oncology in FL, which captures both interpatient and intrapatient heterogeneity, and opens an avenue for drug development.

Statement of significance

We describe the first robust model for functional assessment of primary follicular lymphoma cells, which captures intra- and interpatient heterogeneity of response to immunochemotherapy.

Introduction

Follicular lymphoma (FL) is the second most frequent type of lymphoma. It typically presents as an indolent disease, allowing for a "watch and wait" approach to be taken with some patients who are minimally symptomatic (1). However, most patients will eventually require treatment. The standard of care is a combination of an anti-CD20 monoclonal antibody (rituximab or obinituzumab) with chemotherapy (such as cyclophosphamide, hydroxyadriamycine, vincristine and prednisone (CHOP) or bendamustine) followed by a 2-year maintenance with anti-CD20 (2). Despite impressive results achieved with these treatments (median progression free survival of 10.5 years, 10-year overall survival of 80%) (3), relapse invariably occurs, and lymphoma remains the primary cause of death for these patients (4). It is believed that relapses are caused by cells that are resistant to chemotherapy, but there is currently no data that documents intratumoral heterogeneity regarding treatment response.

Of note, the outcome of FL patients is highly heterogeneous, with a particularly poor prognosis for 20% of the patients experiencing disease progression during the first 24 months of initial immunochemotherapy (POD24) (5). Despite numerous efforts to prospectively identify these patients through analyzing driver mutations (6) or gene expression (7), none have been successful in personalizing first-line treatment. An alternative approach, known as functional precision oncology, which measures the response of living cells to perturbations, has the potential to improve the prediction of response to therapy (8). However, this type of analysis is limited in FL due to the lack of an adequate model, as primary FL cells cannot be grown *in vitro*. A few patient-derived xenograft (PDX) have been established in immunocompromised mice, but these models are time consuming and not suitable for drug testing in mutliple replicates (9). Hence, development of new FL models remains an unmet need to improve patients outcome.

Avian embryos have been recently shown to provide a supportive environment for the growth of human cancer cells, including neuroblastoma, triple negative breast cancer, and melanoma (10–12). Furthermore, as only a small number of cells are needed for each engraftment, multiple experimental conditions can be tested without any pre-amplification of the patient sample thus allowing statistically powerful analysis. In addition, drugs can be administered intravenously in the embryos, making it possible to test drug sensitivity by measuring tumor volume using light sheet microscopy or analyzing exposed tumor cells through single-cell

RNA sequencing (scRNAseq). Here we provide evidence that a new model of FL using PDX in avian embryos (FL-AVI-PDX) captures interpatient heterogeneity regarding treatment response. Additionally, scRNAseq revealed a robust signature of RCHOP induced genes, and an unexpected heterogeneity among lymphoma cells exposed to RCHOP. To validate functionally these findings, we demonstrate that the use of venetoclax to target *BAX*, one of the RCHOP induced genes, could enhance the effects of RCHOP.

Results

Establishment of the patient-derived xenograft avian model of follicular lymphoma (FL-AVI-PDX)

FL cells are highly dependent on their microenvironment to survive (13), which may explain why previous attempts to grow these cells *in vitro* have failed. We hypothesized that signals instructing the hemogenic endothelium to generate hematopoietic stem cells in the avian embryos could offer a supportive microenvironment. To test this hypothesis, we injected FL cells in the aorta-gonado-mesonephros (AGM) embryonic region where hematopoietic stem cells emerge (14). To that end, mechanically dissociated and viably cryopreserved FL samples from diagnostic biopsies were labelled with carboxyfluorescin succinimydil ester (CFSE) in order to be followed *in vivo* and subsequently implanted within the emerging AGM region of series of E2 (Hamburger and Hamilton stage HH15) avian embryos (Figure 1A, Supp. Table 1). All of the primary FL samples tested (n=20) successfully grew in the AGM with 98% (86-100%) of avian embryos with detectable CFSE+ cells 24h after graft (Supp. Table 2). These findings suggest that the emerging AGM region of avian embryos supports primary FL cells survival.

Next we used scRNAseq to evaluate the effect of the engraftment procedure on fourteen FL samples. CFSE-stained cells were collected before engraftment, and CFSE+/hCD45+ cells were collected and sorted by flow cytometry 48 hours after engraftment (Supp. Figure 1A). Among the three protocols of tissue dissociation tested, collagenase combined with actinomycin D allowed the collection of a higher number of cells without inducing a transcriptomic signature associated with dissociation (15,16) (Supp. Figure 1B). Antibody-based barcoding on pooled samples was used to minimize batch effect between cells from the same patient and scRNAseq libraries were processed using the 10X genomics technology. An average of 1455 (range 354 to 3532) and 894 (range 124 to 2776) cells per sample were found to pass the quality control of scRNAseq before and after graft respectively (Supp. Table 3). Before the graft, B cells made up 76% of all cells (range 51% to 91%), with FL cells (characterized by clonal rearrangement of the V(D)J locus and monotypic expression of either kappa or lambda light chain) accounting for 94% of them (Supp. Figure 1C). Other cells included 18% of CD4+ T lymphocytes (range 8% to 44%), including T follicular helper (6%, range 2% to 21%) and other T cells (12%, range 4% to 31%), 4% of CD8+ T lymphocytes (range 0.7% to 12%) and rare myeloid cells such as monocytes (1%, range 0.2% to 2%). The analysis of cells collected 48 hours after the graft showed a significant increase in B cells (average increase of 17%, range -6% to 27%, $p<0.05$) at the expense of microenvironment

cells (Figure 1B). This relative enrichment in tumor cells could be partly due to a higher proportion of actively cycling tumor cells (67.9%) as compared to non-tumor cells (56.3% in S/G2M) at the time of engraftment (Figure 1C, Supp. Table 3).

Unsupervised analysis revealed that the transcriptomic diversity was primarily caused by cell type (B cells vs non-tumor cells) and experimental condition (pre vs. post-graft) (Figure 1D), which together explained 28% of the variability of the dataset by principal component analysis (Supp. Figure 1D). The intersection of both single cell and pseudo-bulk analysis identified a list of differentially expressed genes (DEG) between pre and post-graft B cells (see methods and Supp. Figure 1E) (17). Gene set enrichment analysis (GSEA) identified an upregulation of metabolic and pro-survival pathways (glycolysis, oxidative metabolism, mTORC1 and MYC) in post-graft samples, suggesting that the early AGM region provides a nurturing environment for FL cells (Figure 1E). Interestingly, we also identified heterogeneity among the cells collected after graft. Unsupervised clustering identified a cluster representing 13% of total cells with a high level of expression of glycolysis and hypoxia signature (Figure 1F), potentially due to engraftment in hypoxic areas of the embryos.

In conclusion, the data shows that the AGM region in avian embryos provides a favorable microenvironment for primary FL cells, which prompted us to test whether it is a suitable model to examine the therapeutic response of FL.

Figure 1

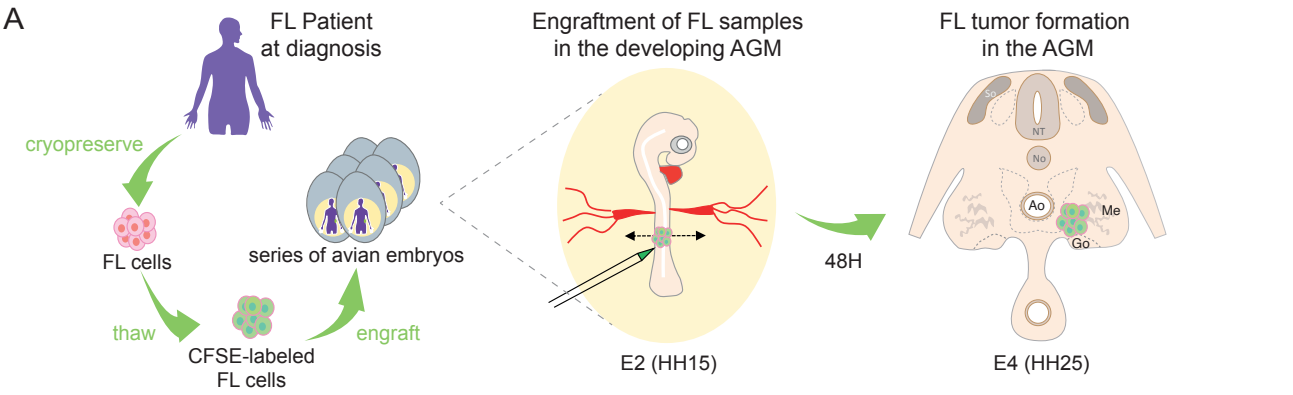
A
FL Patient
at diagnosis
cryopreserve
FL cells
thaw
CFSE-labeled
FL cells
series of avian embryos
engraft
Engraftment of FL samples
in the developing AGM
E2 (HH15)
48H
FL tumor formation
in the AGM
E4 (HH25)
So
NT
No
Ao
Me
Go

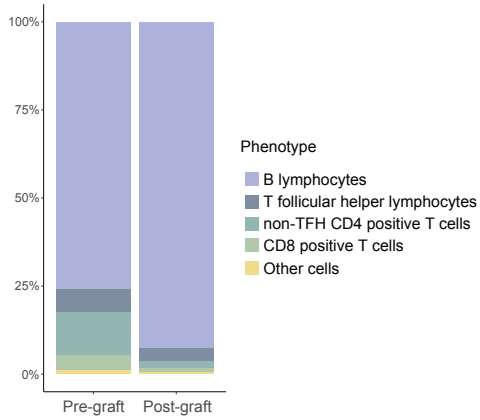
B
100%
75%
50%
25%
0%
Pre-graft
Post-graft
Phenotype
B lymphocytes
T follicular helper lymphocytes
non-TFH CD4 positive T cells
CD8 positive T cells
Other cells

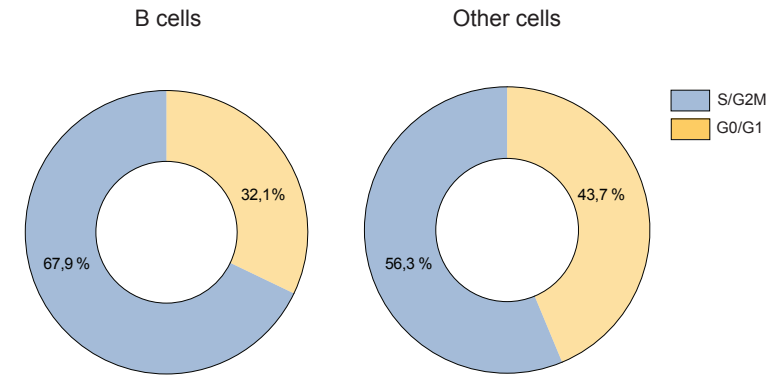
C
B cells
Other cells
32,1%
67,9 %
43,7 %
56,3 %
S/G2M
G0/G1

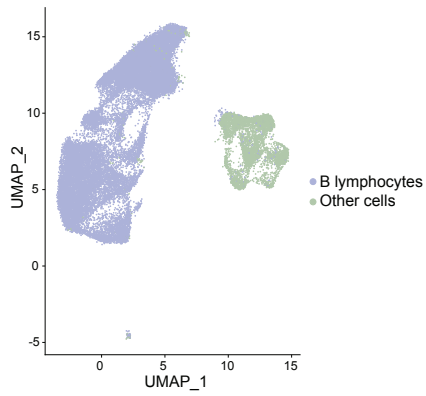
D
UMAP_2
UMAP_1
B lymphocytes
Other cells

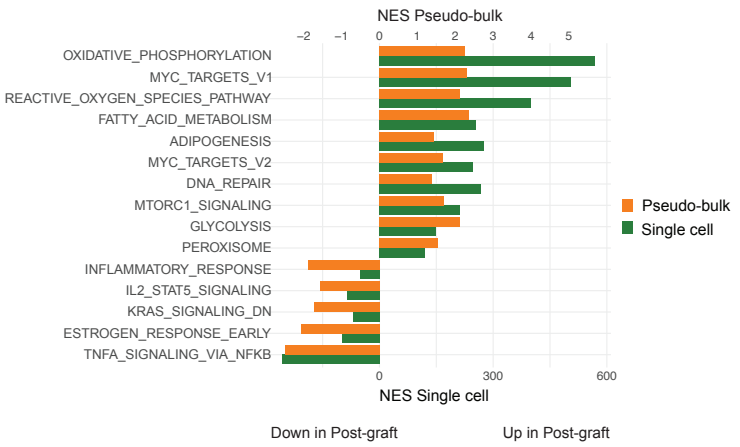
E
NES Pseudo-bulk
OXIDATIVE_PHOSPHORYLATION
MYC_TARGETS_V1
REACTIVE_OXYGEN_SPECIES_PATHWAY
FATTY_ACID_METABOLISM
ADIPOGENESIS
MYC_TARGETS_V2
DNA_REPAIR
MTORC1_SIGNALING
GLYCOLYSIS
PEROXISOME
INFLAMMATORY_RESPONSE
IL2_STAT5_SIGNALING
KRAS_SIGNALING_DN
ESTROGEN_RESPONSE_EARLY
TNFA_SIGNALING_VIA_NFKB
NES Single cell
Pseudo-bulk
Single cell
Down in Post-graft
Up in Post-graft

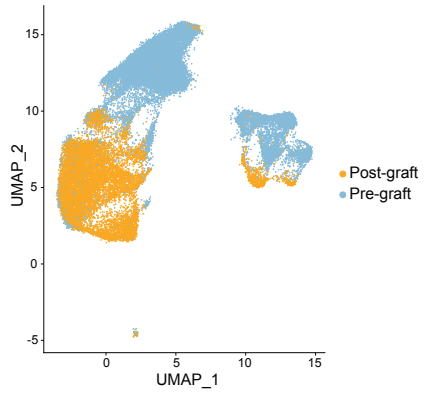
UMAP_2
UMAP_1
Post-graft
Pre-graft

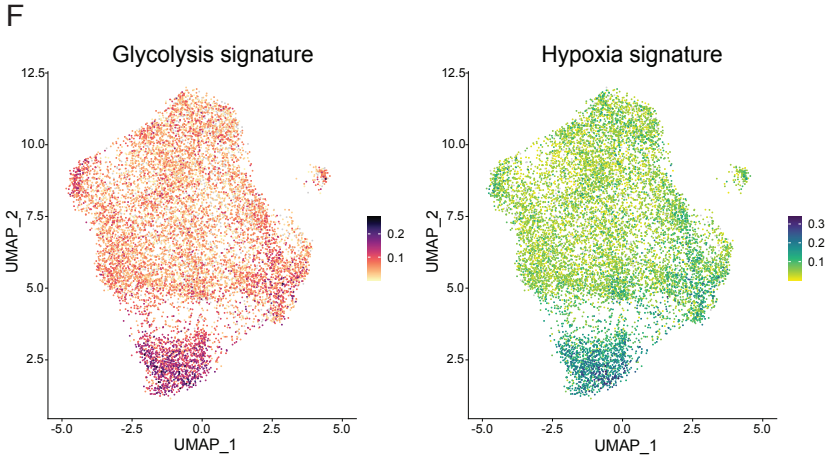
F
Glycolysis signature
Hypoxia signature
UMAP_2
UMAP_1

<u>Figure 1:</u> Establishment of the patient-derived xenograft avian model of follicular lymphoma (FL-AVI-PDX).

(A) Schematic representation of the FL-AVI-PDX model. **(B)** Analysis of cell composition before (pre-graft) and after (post-graft) graft based on scRNAseq data. **(C)** Proportion of S/G2/M or G0/G1 cells among B cell or non-B cells in pre-graft samples. **(D)** Uniform Manifold approximation and projection (UMAP) representation of the unsupervised analysis of scRNAseq data from fourteen patients. Individual cells are labeled by cell type (top) or by experimental condition (bottom). **(E)** Gene set enrichment analysis of differentially expressed genes in pseudo-bulk (orange) or single cell (green) analysis showing the up and down-regulated pathways in post-graft B cells. **(F)** Intensity of expression of the glycolysis (left) and hypoxia (right) signatures by post-graft B cells.

AGM: Aorta-gonad-mesonephros; DA: dorsal aorta; HSC: hematopoietic stem cells, FL: follicular lymphoma, E2/4: Embryonic day 2/4; NES: normalized enrichment score

Supp. Figure 1

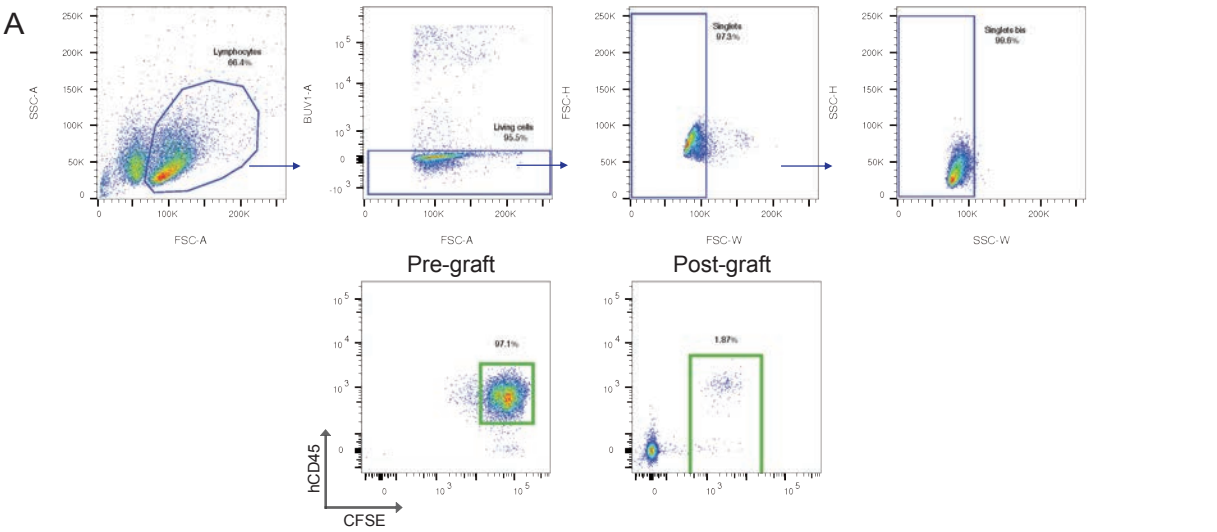

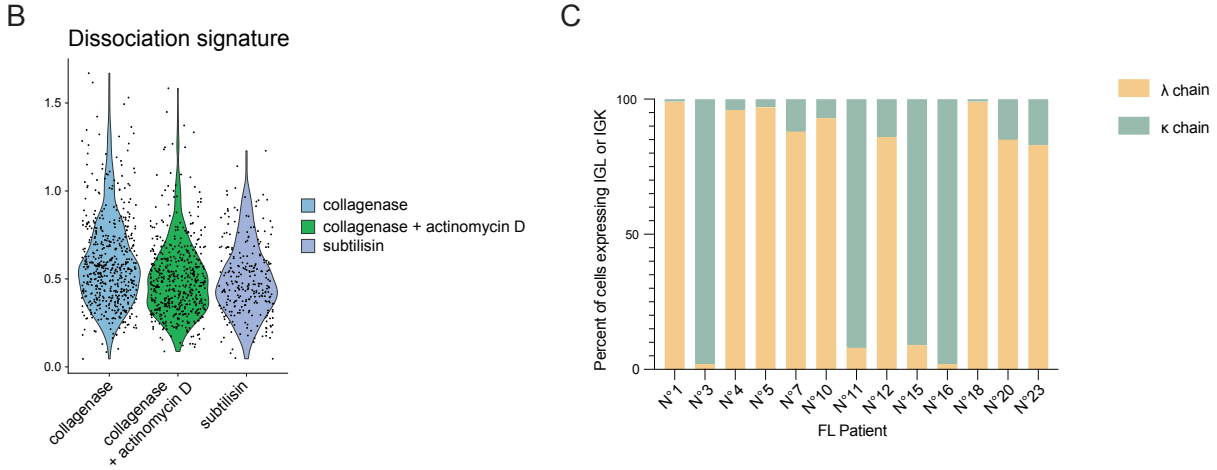

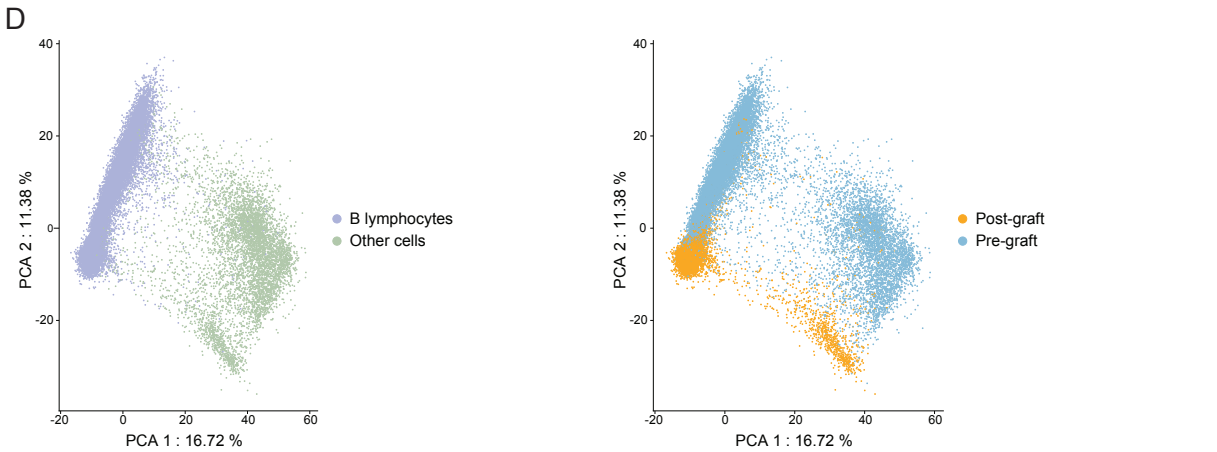

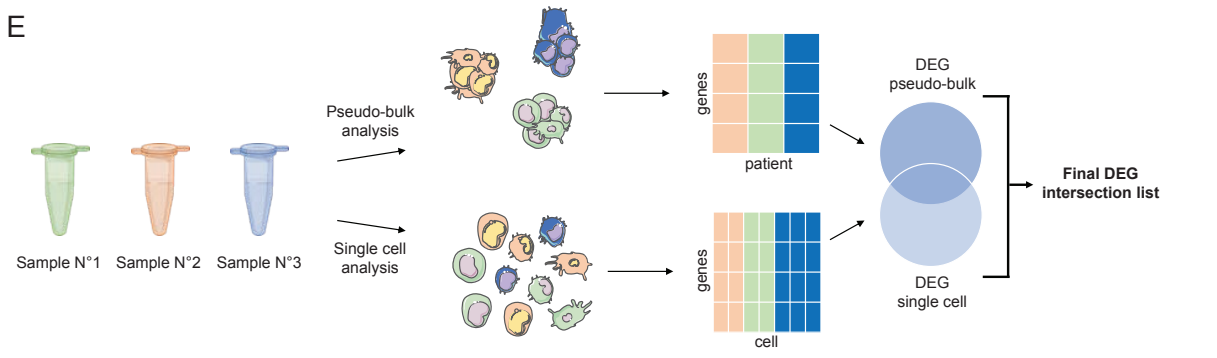

<u>Supp. Figure 1:</u> Establishment of the patient-derived xenograft avian model of follicular lymphoma (FL-AVI-PDX).

(A) Flow cytometry gating strategy for human CD45+ CFSE+ cell sorting. The maximum number of cells were sorted for the post-graft condition, and an equivalent number of cells were sorted for the pre-graft fraction to avoid imbalance in the number of cells per condition. **(B)** Expression of the dissociation signature by cells after graft with three different protocols. **(C)** Percentage of cells expressing IGL or IGK light chain in each sample (n= 13). **(D)** Principal component analysis (PCA) representation of the pre- and post-graft scRNAseq data. Individual cells are labeled according to their phenotype (left panel) or to experimental condition (right panel). **(E)** Schematic representation of the analytical strategy used to identify the differentially expressed gene list based on single cell and pseudo-bulk methods.

FL-AVI-PDX captures clinical heterogeneity of response to RCHOP

In order to assess the ability of the FL-AVI-PDX model to capture interpatient heterogeneity of therapeutic response, we exposed the engrafted embryos to RCHOP, a commonly prescribed first-line therapy for FL patients (2). The maximal tolerated dose (MTD) of the RCHOP combination, used with the same stoichiometry between each drug as in clinics, was determined after a single intravenous injection of the combination (Supp. Table 4). Toxicity of each dose was assessed by measuring the growth (body surface area (BSA)) and survival of avian embryos (11,12). The MTD of RCHOP (rituximab 5.13 mg/kg, cyclophosphamide 10.25 mg/kg, hydroxyadriamycine (doxorubicin) 0.69 mg/kg, vincristine 0.02 mg/kg, prednisone 0.54 mg/kg) was associated with a 86% survival rate and did not impact the embryonic BSA as compared to excipient-treated embryos (Supp. Figure 2A). The pharmacokinetic profiles of the RCHOP components were also analyzed in avian embryos blood at different time points after RCHOP intravenous injection (0.5, 3 and 8 hours). All drugs tested (rituximab, cyclophosphamide, hydroxyadriamycine, and vincristine) were detectable with a concentration peak at 0.5h followed by a slow decrease over time (Figure 2A). Compounds were detected in avian embryos at concentration 10-100 times lower than those observed in lymphoma patients (18), yet their pharmacokinetic profiles were similar (Supp. Figure 2B). These findings suggest that the RCHOP regimen can be safely given to avian embryos, and its pharmacokinetic profile is suitable for investigating the therapeutic response of FL.

We then used FL-AVI-PDX models from the twenty patients treated initially with RCHOP and rituximab maintenance, including 9 poor responders with FL progression during the first 24 months (POD24) and 11 good responders with long progression free survival (Supp. Table 1). Twenty-four hours after engraftment, FL-bearing avian embryos were randomly treated by intravenous injection RCHOP or excipient. The embryos were harvested after an additional 24 hours (HH25) for measurement of tumor volumes based on CFSE fluorescence using light sheet microscopy (Figure 2B). RCHOP consistently reduced the mean tumor volume in FL-AVI-PDX from the good responder patients but not in FL-AVI-PDX from poor responder patients (Figure 2C). Accordingly, the mean tumor volume reduction from all the samples was significantly higher in FL-AVI-PDX from good responders compared to poor responders (mean tumor volume reduction 35% vs. -2%, p=0.0001) (Figure 2D, Supp. Table 2). To further explore this result beyond the binary categorization of clinical response, we evaluated whether tumor volume reduction could predict progression free survival using a Cox model (Supp. Figure 2C). Multivariate analysis showed that tumor volume reduction, and not FL

International Prognostic Index (FLIPI), is an independent prognostic predictor in this cohort (hazard ratio 0.32, range 0.15-0.67, p=0.003) (Figure 2E). Altogether, these data show that the FL-AVI-PDX heterogeneous response to RCHOP is correlated to clinical outcome.

Figure 2

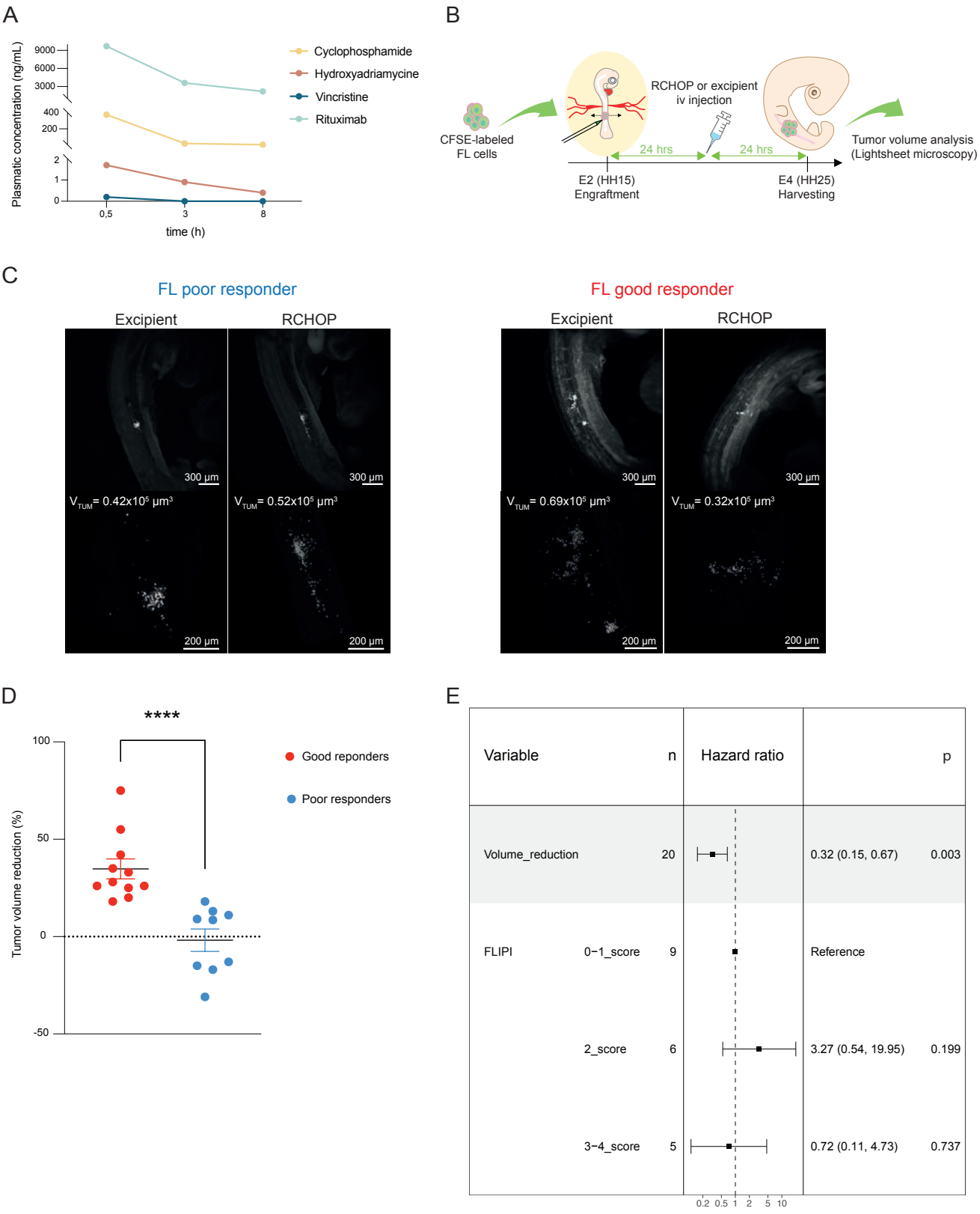
A
Plasmatic concentration (ng/mL)
9000
6000
3000
400
200
2
1
0
0,5
3
8
time (h)
Cyclophosphamide
Hydroxyadriamycine
Vincristine
Rituximab
B
CFSE-labeled
FL cells
RCHOP or excipient
iv injection
24 hrs
24 hrs
E2 (HH15)
Engraftment
E4 (HH25)
Harvesting
Tumor volume analysis
(Lightsheet microscopy)
C
FL poor responder
Excipient
RCHOP
300 µm
V_TUM= 0.42x10⁵ µm³
V_TUM= 0.52x10⁵ µm³
200 µm
FL good responder
Excipient
RCHOP
V_TUM= 0.69x10⁵ µm³
V_TUM= 0.32x10⁵ µm³
D
****
Tumor volume reduction (%)
100
50
0
-50
Good reponders
Poor responders
E
Variable
n
Hazard ratio
p
Volume_reduction
20
0.32 (0.15, 0.67)
0.003
FLIPI
0−1_score
9
Reference
2_score
6
3.27 (0.54, 19.95)
0.199
3−4_score
5
0.72 (0.11, 4.73)
0.737
0.2
0.5
1
2
5
10

<u>Figure 2:</u> FL-AVI-PDX captures clinical heterogeneity of response to RCHOP

(A) Plasmatic concentration of rituximab, cyclophosphamide hydroxyadriamycine and vincristine after a single intravenous injection of RCHOP MTD in avian embryos. **(B)** Schematic representation of the experimental procedure used to evaluate the effects of RCHOP on FL-AVI-PDX. **(C)** Representative example of light sheet microscopy imaging after exposure to RCHOP or excipient in a poor (left) and good responder patient (right) in whole cleared embryos (upper panels) and precise quantification of tumor volumes (lower panels). **(D)** Mean percentage of tumor volume reduction achieved with RCHOP in FL-AVI-PDX from good and poor responder patients. Error bars indicate SEM. **** p value <0.0001 (Mann-Whitney test). **(E)** Forest plot showing hazard ratios and 95% confidence intervals for progression-free survival in multivariate analysis.

Supp. Figure 2

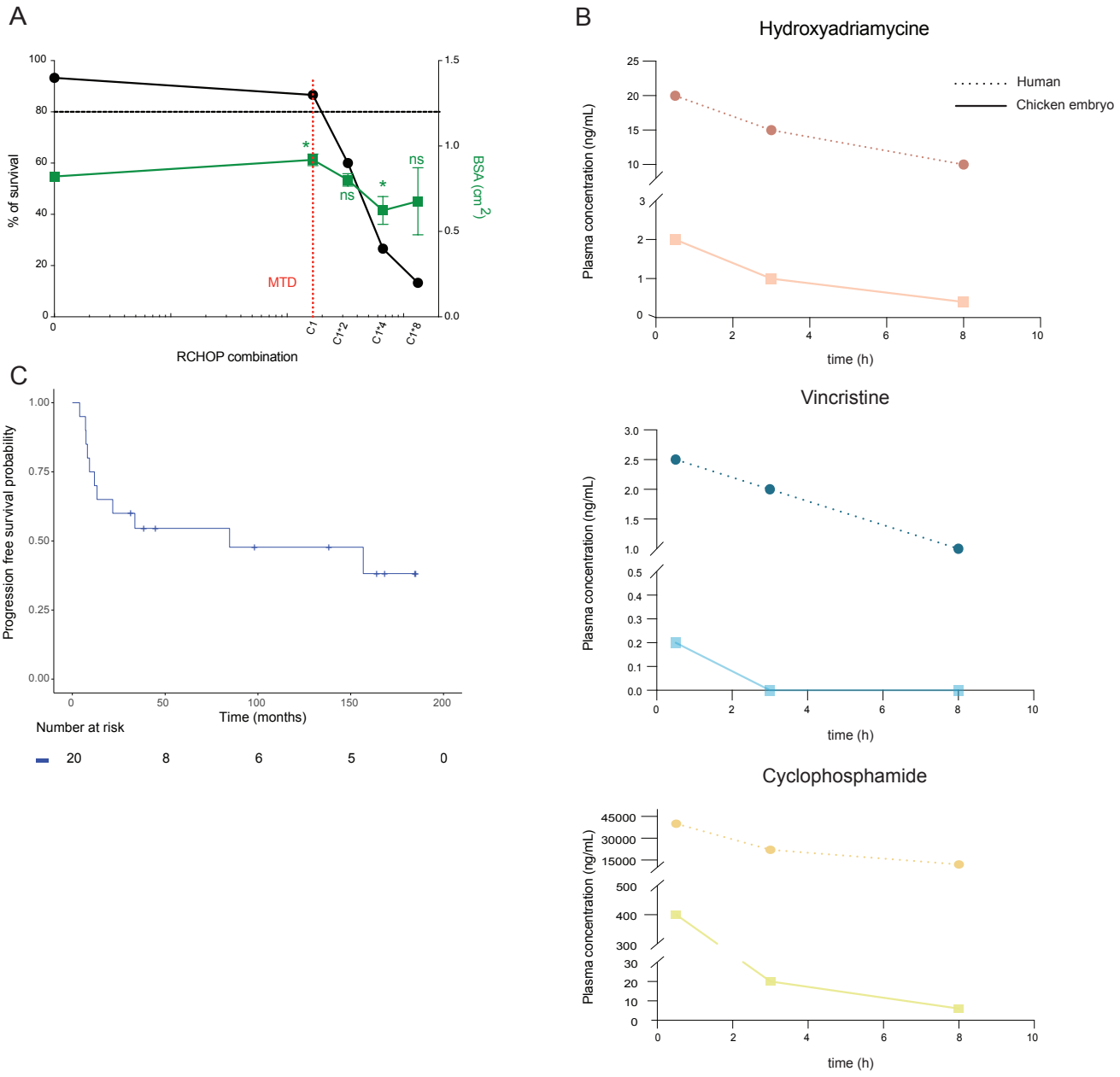

<u>Supp. Figure 2:</u> FL-AVI-PDX captures clinical heterogeneity of response to RCHOP.

(A) Survival rate and mean body surface area (BSA) of avian embryos injected with increasing doses of RCHOP combination. The maximum tolerated dose (MTD) is the higher dose with no impact on BSA and a survival rate greater than 80%. Data are expressed as mean +/- SEM, * $p<0.05$ (Mann-Whitney test). **(B)** Comparison of the pharmacokinetics of cyclophosphamide, hydroxyadriamycin and vincristine in human (data from (1)) (dotted line) and in avian embryos (continuous line). **(C)** Kaplan-Meier progression free survival curve of the whole cohort (n= 20).

FL-AVI-PDX reveals a transcriptomic signature of response to RCHOP in primary FL cells

The knowledge about the mechanisms of action of chemotherapies on FL cells is mostly derived from cancer cell lines, and no data have been generated on primary cells so far. Therefore, we further used the FL-AVI-PDX model to explore the mechanisms of response of primary FL cells to RCHOP by using scRNAseq. We compared B cells from fourteen FL-AVI-PDX collected after graft and exposed to either RCHOP or vehicle, by combining both single cell and pseudo-bulk strategies in order to mitigate the batch sample effect observed in single cell analysis. A list of 21 genes upregulated after RCHOP exposure was identified by both methods (Figure 3A, Supp. Table 5). Among these genes are key effector of p53 response and/or apoptosis such as *DDB2, PVT1, BAX* and *BBC3* (*PUMA*). We confirmed the induction of some of these genes (*BAX, RPS27L*, *RPS19* but not *SRSF3*) after RCHOP exposure by quantitative PCR in a germinal center derived lymphoma cell line (SUDHL-4) (Supp. Figure 3A). We then treated this line with each drug separately, to analyze their contribution to the transcriptomic modifications identified in response to RCHOP. Except for *RPS27L* whose induction was only observed with hydroxyadriamycine, the induction of the other genes was not observed with any single drug, suggesting that complex synergies drive the observed transcriptomic modifications (Supp. Figure 3B).

Intratumoral heterogeneity is recognized as an important factor driving resistance to cancer treatment, which is especially important in FL where relapses occur invariably. To evaluate the heterogeneity of response to RCHOP among cancer cells, we assessed the level of expression of the RCHOP signature in the different B cells clusters identified by unsupervised clustering strategies. Interestingly, we found that a specific cluster (cluster #8) strongly expressed the RCHOP signature. We also identified a cluster (cluster #4) overexpressing this signature in samples stressed only by the graft procedure, albeit with lower magnitude as compared to RCHOP exposed samples, and no such cluster was found in pregraft samples. (Figure 3B). Cluster #8 was present in each patient's sample, representing 3-12% of the cells, and its relative size was not different between samples from good or poor responders (Figure 3C, Supp. Figure 3C). Further analysis using GSEA showed that this cluster was significantly enriched in transcriptomic signatures of apoptosis, p53 activation, cell cycle checkpoint, UV response and TNF alpha signaling (Figure 3D). Unexpectedly, expression of mitochondrial genes, which is commonly used as a proxy of apoptotic process, was significantly lower in this cluster (Figure 3E).

Altogether, our findings uncover a transcriptomic signature of response to RCHOP in primary FL cells and highlight heterogeneity in the level of induction of this signature among primary FL cells. To further validate the FL-AVI-PDX model, we investigated whether we could identify new treatment approaches in FL based on the transcriptomic signature of response to RCHOP.

Figure 3

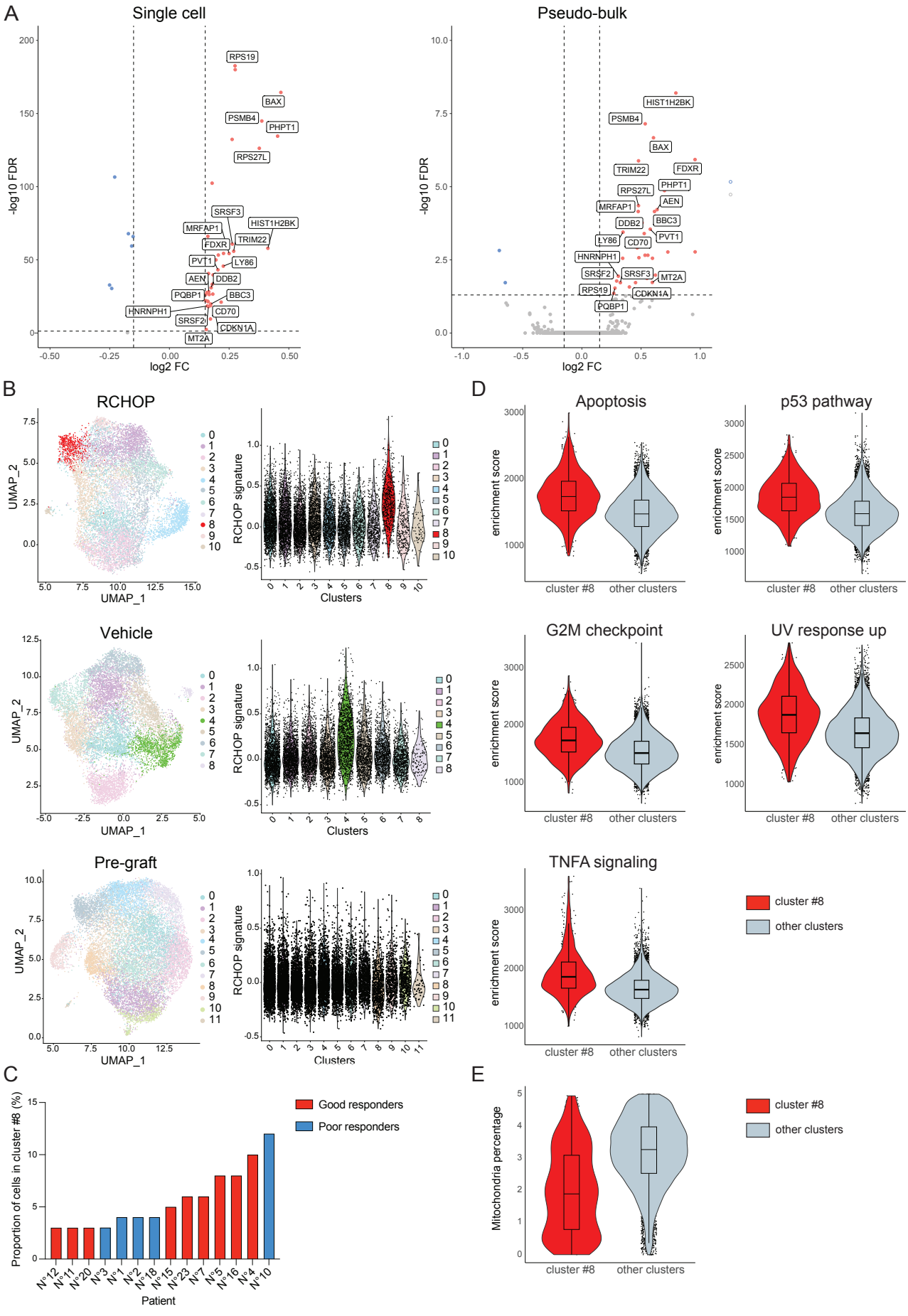
A
Single cell
Pseudo-bulk
-log10 FDR
log2 FC
RPS19
BAX
PSMB4
PHPT1
RPS27L
SRSF3
MRFAP1
HIST1H2BK
FDXR
TRIM22
PVT1
LY86
AEN
DDB2
PQBP1
BBC3
HNRNPH1
CD70
SRSF2
CDKN1A
MT2A
B
RCHOP
Vehicle
Pre-graft
UMAP_1
UMAP_2
RCHOP signature
Clusters
C
Good responders
Poor responders
Proportion of cells in cluster #8 (%)
Patient
N°12
N°11
N°20
N°3
N°1
N°2
N°18
N°15
N°23
N°7
N°5
N°16
N°4
N°10
D
Apoptosis
p53 pathway
G2M checkpoint
UV response up
TNFA signaling
enrichment score
cluster #8
other clusters
E
Mitochondria percentage

<u>Figure 3:</u> FL-AVI-PDX reveals a transcriptomic signature of response to RCHOP in primary FL cells

(A) Volcano plot showing the differentially expressed genes by B cells exposed to RCHOP as determined by single cell (left panel) and pseudo bulk method (right panel). The 21 up-regulated genes identified by both methods are labeled in red. **(B)** Uniform Manifold Approximation and Projection (UMAP) representation of the scRNAseq analysis of B cells exposed *in ovo* to RCHOP (upper panel), to vehicle (central panel) or before graft (lower panel) and intensity of the expression of the RCHOP signature in each cluster for each corresponding condition. **(C)** Percentage of cells belonging to cluster #8 for each sample (n=14, including 9 good responders (red) and 5 poor responders (blue)) **(D)** GSEA analysis of cells belonging to cluster #8 as compared to cells from all other clusters in RCHOP-exposed cells (FDR < 0.05). (**E**) Violin plot representation of the percentage of genes encoded by the mitochondrial genome in cells belonging to cluster #8 as compared to cells from all other clusters in RCHOP-exposed cells.

Supp. Figure 3

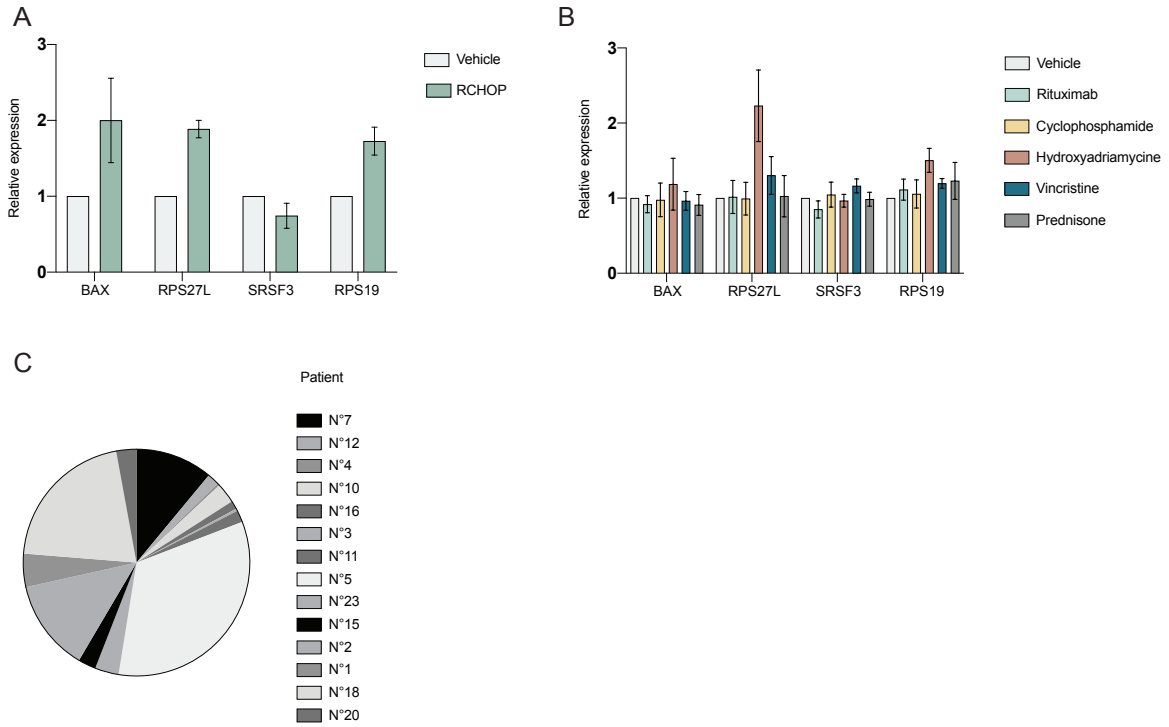

<u>Supp. Figure 3:</u> FL-AVI-PDX reveals a transcriptomic signature of response to RCHOP in primary FL cells

(A-B) Quantitative RT-PCR assessment of the relative expression of BAX, RPS27L, SRSF3 and RPS19 (included in the RCHOP signature) normalized on GAPDH expression in the SUDHL-4 cell line exposed to vehicle or RCHOP overnight **(A)** or to each of the five compounds individually **(B)**. **(C)** Sample of origin of cells of cluster 8 (n= 590 single cells).

BAX is a targetable effector of RCHOP in FL

BAX was found to be overexpressed after RCHOP exposure in primary cells, and especially in cluster #8 cells, as well as in the SUDHL-4 cell line (Figure 4A, Supp. Figure 3A). *BAX* interacts with BH3-only proteins such as BAD, BID, or BIM, and forms homo- or hetero-oligomers (with BAK) in the outer mitochondrial membrane, causing cytochrome c release and apoptotic cell death through the process of mitochondrial outer membrane permeabilization (MOMP). Its activation is inhibited by pro-survival members of the BCL2 family such as BCL2 itself, which is overexpressed in FL due to the t(14;18) translocation (19).

First, we examined the effect of *BAX* inactivation on RCHOP-induced apoptosis. Using CRISPR-Cas9, we deleted *BAX* in the SUDHL-4 cell line with two different sgRNA (Supp. Figure 4A). The $BAX^{-/-}$ cell lines were less sensitive to RCHOP compared to the wild type cells expressing a non-targeting sgRNA (Figure 4B). We hypothesized that increasing the level of *BAX* or its activation might, on the contrary, further enhance the effects of RCHOP. To test this hypothesis we used venetoclax, an FDA-approved BCL2 inhibitor that indirectly increases *BAX* activity (20,21) (Supp. Figure 4B). As expected, $BAX^{-/-}$ cells were resistant to venetoclax (Supp. Figure 4C). The combination of RCHOP and venetoclax resulted in an additive effect on cell death induction in the SUDHL-4 lymphoma cell line, in a *BAX*-dependent manner (Figure 4C).

To further examine the potential benefits of targeting *BAX* to enhance the efficacy of RCHOP, we compared the RCHOP-venetoclax combination to RCHOP or venetoclax alone using the FL-AVI-PDX model. We first established the MTD of venetoclax when used alone or in combination with RCHOP. The MTD of intravenous venetoclax as a single agent was 172 mg/kg, but it decreased to 57 mg/kg when combined with RCHOP (Supp. Figure 4D, Supp. Figure 4E and Supp. Table 6). We used this dose to assess the efficacy of the RCHOP-venetoclax combination in six primary FL samples from good (n=4) or poor responders (n=2) to RCHOP (Supp. Table 1). As expected, the FL-AVI-PDX established from poor responder patients did not respond to RCHOP alone, but a pronounced response was observed with the addition of venetoclax (Figure 4D). The better efficacy of the RCHOP-venetoclax was confirmed in the whole cohort (mean tumor volume reduction 52.5% vs. 16.5% $p<0.05$) (Figure 4E). These findings demonstrate that the FL-AVI-PDX model can be used to identify and validate combination therapies.

Figure 4

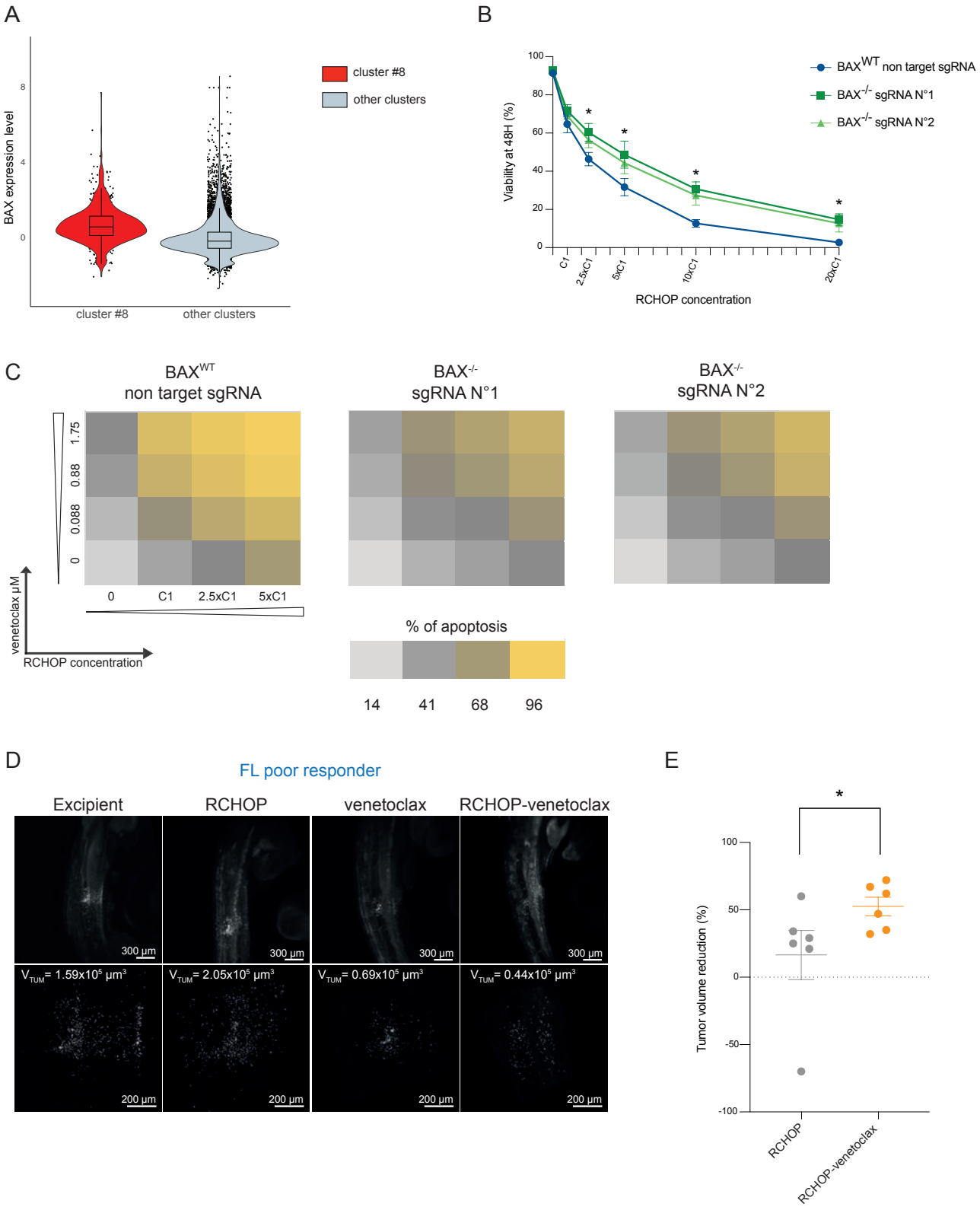
A
BAX expression level
cluster #8
other clusters
cluster #8
other clusters
B
Viability at 48H (%)
BAXWT non target sgRNA
BAX-/- sgRNA N°1
BAX-/- sgRNA N°2
C1
2.5xC1
5xC1
10xC1
20xC1
RCHOP concentration
C
BAXWT
non target sgRNA
BAX-/-
sgRNA N°1
BAX-/-
sgRNA N°2
venetoclax µM
RCHOP concentration
0
C1
2.5xC1
5xC1
% of apoptosis
14
41
68
96
D
FL poor responder
Excipient
RCHOP
venetoclax
RCHOP-venetoclax
300 µm
200 µm
E
Tumor volume reduction (%)
RCHOP
RCHOP-venetoclax

Figure 4: ***BAX*** **is a targetable effector of RCHOP in FL**

(A) Violin plot representation of *BAX* level expression in cells belonging to cluster #8 as compared to cells from all other clusters in RCHOP-exposed cells. **(B)** Proportion of viable SUDHL-4 cells ($BAX^{-/-}$ with two different sgRNA targeting *BAX* or BAX^{WT} with a non-target sgRNA) after 48h exposure to increasing doses of RCHOP. Error bars indicate SD. *p Val<0.05 (Wilcoxon test). **(C)** Proportion of apoptotic SUDHL-4 cells ($BAX^{-/-}$ with two different sgRNA targeting *BAX* or BAX^{WT} with a non-target sgRNA) after a 48h-exposure to increased doses of RCHOP and venetoclax combinations. **(D)** Example of light sheet imaging for one embryo of each condition in whole cleared embryos (upper panels) and precise quantification of tumor volumes for analysis (lower panels) for a patient with poor response to RCHOP. **(E)** Mean percentage of tumor volume reduction observed after RCHOP or RCHOP-venetoclax treatment of FL-AVI-PDX (n=6). Error bars indicate SEM, * p<0.05 (Mann-Whitney test)**.**

Supp. Figure 4

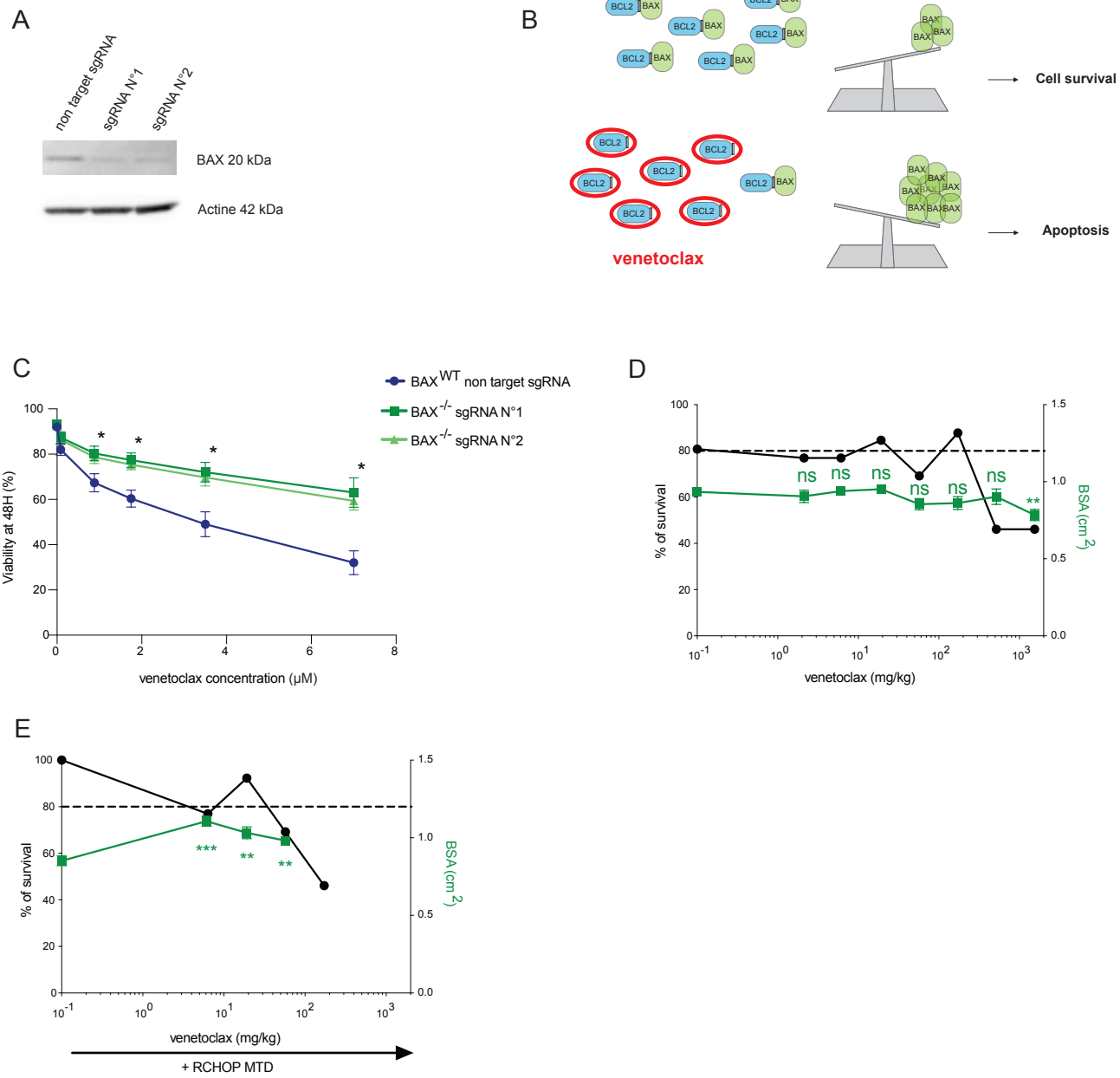

Supp. Figure 4: BAX is a targetable effector of RCHOP in FL

(A) Western blot analysis of BAX protein levels in SUDHL-4 cells ($BAX^{-/-}$ with two different sgRNA targeting BAX or BAX^{WT} with a non-target sgRNA). **(B)** Schematic representation of the mechanism of action of venetoclax. **(C)** Proportion of viable (annexin V negative) SUDHL-4 cells ($BAX^{-/-}$ with two different sgRNA targeting BAX or BAX^{WT} with a non-target sgRNA) after 48h exposure to increasing doses of venetoclax (µM). Error bars indicate SD. *p Val<0.05 (Wilcoxon test). **(D)** Survival rate and mean body surface area (BSA) of avian embryos injected with increasing doses of venetoclax. The maximum tolerated dose (MTD) is the higher dose with no impact on BSA and a survival rate greater than 80%. Data are expressed as mean +/- SEM, **p Val <0.005, ns not significant (Mann-Whitney test). **(E)** Survival rate and mean body surface area (BSA) of avian embryos injected with increasing doses of venetoclax combined with the MTD of RCHOP. **p Val <0.005, ***p Val <0.0001 (Mann-Whitney test).

Discussion

For decades, researchers have focused on cell lines as models for cancer. However, with the progressive recognition of the ecological complexity of cancer (22), the development of more relevant models has become necessary. Patient-derived xenografts in immunocompromised mice have been a major breakthrough, allowing for direct evaluation of drug therapies in a more physiological setting (9). However, this strategy has limitations for B cell lymphomas, particularly for FL, which grow only occasionally in these models, and have a long latency of development (23). Here we report experimental data supporting the use of avian embryos as an alternative recipient for FL PDX. This model allowed for successful engraftment of all samples tested, with a large number of replicates, providing robust statistical power to test therapeutic strategies. Using RCHOP as a proof of concept, we observed a clear correlation between response to RCHOP *in ovo* and clinical outcome, which demonstrates that clinically relevant information can be derived from functional testing of FL in this model. As almost all FL patients achieve complete clinical response after 6 courses of RCHOP, the observation of a significant difference of response to RCHOP *in ovo* was unexpected. We hypothesize that this differential effect on bulk tumor reduction is due to the low drug concentrations achieved in avian embryos, which may reveal subtle differences in chemosensitivity. Other limitations of the model are the absence of complement proteins in avian embryos at the early stages of development, which might limit the activity of rituximab (24), and short experiment duration. Further research is necessary to determine if longer duration of graft could provide a deeper understanding of inter-patient variability. Another potential development of this model as a predictive biomarker would require prospective evaluation in large patient cohorts.

The FL-AVI-PDX model also allows to collect back cells from the grafted tumors, which provides a unique opportunity to examine the effects of treatments on primary tumor cells. We describe here a list of 21 genes that were upregulated after RCHOP exposure, including genes related to the known mechanisms of action of chemotherapy. Notably, not all of these genes were activated after RCHOP treatment of a cell line, emphasizing the value of using FL PDX models to fill in the knowledge gaps. As a proof of concept of the usefulness of this model, we performed functional validation of the role of *BAX* in RCHOP-induced apoptosis. This led us to investigate the potential benefits of combining venetoclax with RCHOP, which was found to be additive in both cell lines and primary FL *in ovo*, including in samples from poor responder patients. Of note, the RCHOP-venetoclax combination has been already evaluated in the CAVALLI phase 1b study which included 10 FL patients, and showed acceptable safety profile and a complete remission rate of 70% (25). The observed

heterogeneity in the treatment response *in ovo* suggests that the results at the cohort level might underestimate the potential benefit of this combination for subgroups of patients such as those predicted to poorly respond to RCHOP.

In addition to its use as a platform for preclinical development in FL treatments, the FL-AVI-PDX model revealed intratumoral heterogeneity in response to RCHOP. In all samples we identified a cluster of cells (cluster #8) with a high expression of the RCHOP signature. This signature reveals the activation of stress response (such as the p53 pathway), which is also heterogeneously expressed in engrafted samples not exposed to chemotherapy, albeit to a lesser extent. Intriguingly, the expression of mitochondrial genes, which are usually considered as a proxy of the apoptotic process in single cell RNA-seq studies, was lower in cells belonging to cluster #8. This raises the hypothesis that these cells may be able to withstand strong proapoptotic gene expression due to their low mitochondrial content (26). Further study through the isolation of these cells is needed to confirm this hypothesis and assess their role in relapse after immunochemotherapy.

Altogether, the FL-AVI-PDX model is a unique opportunity to develop functional oncology strategies in FL, to further increase our understanding of this disease and improve patient outcome.

Materials and methods

Patient Samples

Diagnostic biopsy samples from FL patients treated with RCHOP followed by rituximab maintenance were mechanically dissociated and cryopreserved in 10% fetal calf serum (FCS) and dimethylsulfoxyde (DMSO). All patients gave their written consent for the use of their samples in research protocol. Electronic health records were reviewed to determine the main characteristics of the patients at diagnosis and their outcome (Supp. Table 1). Progression free survival (PFS) was defined as the delay between treatment initiation and relapse, progression or death.

In ovo xenograft of Follicular Lymphoma samples (FL-AVI-PDX)

The AVI-PDX procedure is a registered and patented trademark of OncoFactory SAS, an ERBC company.

After thawing, FL cells were labeled with an 8µM Carboxy Fluorescin Succinimidyl Ester (CFSE) solution (Life technologies Carlsbad, California) and a fraction of CFSE-labeled cells was frozen at this step (pre-graft experimental condition). Stage HH14 avian embryos were grafted with 1000-2000 cells in the presumptive AGM region, with a glass capillary connected to a pneumatic pico-pump (PV820, World precision instruments, Sarasota, Florida) under a fluorescent stereomicroscope. Grafted eggs were incubated at 38.5°C in a humidified incubator until HH25 stage, as already published (10,11).

FL-AVI-PDX analysis

For tumor volume measurement, PFA-fixed HH25 embryos were cleared using an adapted Ethyl-Cinnamate protocol (11) and imaged using the UltraMicroscope SPIM (Miltenyi Biotec). 3D-images and volumetric analysis were built using Imaris™ software with the "Surface" module adjusted on CFSE fluorescence.

Alternatively, FL tumors were microdissected under a stereomicroscope and dissociated using collagenase and actinomycin D (see supplemental materials and methods). Dissociated cells were frozen and then thawed, incubated with anti hCD45 and hashtag antibodies (Biolegend, San Diego, CA), and sorted on a FACS Aria III cytometer (Becton Dickinson). Sorted cells were immediately loaded into the Chromium Controller (10X genomics, Pleasanton, California) and libraries were prepared according to the manufacturer's instructions. After sequencing, BCL files were converted to FASTQ using CellRanger mkfastq and aligned on the GRCh38 human genome using CellRanger software.

Detailed description of bioinformatics analyses and wet lab experiments are provided in the supplemental material and method section.

References

1. Ardeshna KM, Smith P, Norton A, Hancock BW, Hoskin PJ, MacLennan KA, et al. Long-term effect of a watch and wait policy versus immediate systemic treatment for asymptomatic advanced-stage non-Hodgkin lymphoma: a randomised controlled trial. Lancet. 2003;362:516–22.

2. Salles G. How do I sequence therapy for follicular lymphoma? Hematology. 2020;2020:287–94.

3. Bachy E, Seymour JF, Feugier P, Offner F, López-Guillermo A, Belada D, et al. Sustained Progression-Free Survival Benefit of Rituximab Maintenance in Patients With Follicular Lymphoma: Long-Term Results of the PRIMA Study. Journal of Clinical Oncology. 2019;37:2815–24.

4. Sarkozy C, Maurer MJ, Link BK, Ghesquieres H, Nicolas E, Thompson CA, et al. Cause of Death in Follicular Lymphoma in the First Decade of the Rituximab Era: A Pooled Analysis of French and US Cohorts. Journal of Clinical Oncology. 2019;37:144–52.

5. Casulo C, Byrtek M, Dawson KL, Zhou X, Farber CM, Flowers CR, et al. Early Relapse of Follicular Lymphoma After Rituximab Plus Cyclophosphamide, Doxorubicin, Vincristine, and Prednisone Defines Patients at High Risk for Death: An Analysis From the National LymphoCare Study. Journal of Clinical Oncology. 2015;33:2516–22.

6. Pastore A, Jurinovic V, Kridel R, Hoster E, Staiger AM, Szczepanowski M, et al. Integration of gene mutations in risk prognostication for patients receiving first-line immunochemotherapy for follicular lymphoma: a retrospective analysis of a prospective clinical trial and validation in a population-based registry. The Lancet Oncology. 2015;16:1111–22.

7. Huet S, Tesson B, Jais J-P, Feldman AL, Magnano L, Thomas E, et al. A gene-expression profiling score for prediction of outcome in patients with follicular lymphoma: a retrospective training and validation analysis in three international cohorts. The Lancet Oncology. 2018;19:549–61.

8. Letai A, Bhola P, Welm AL. Functional precision oncology: Testing tumors with drugs to identify vulnerabilities and novel combinations. Cancer Cell. 2022;40:26–35.

9. Townsend EC, Murakami MA, Christodoulou A, Christie AL, Köster J, DeSouza TA, et al. The Public Repository of Xenografts Enables Discovery and Randomized Phase II-like Trials in Mice. Cancer Cell. 2016;30:183.

10. Delloye-Bourgeois C, Bertin L, Thoinet K, Jarrosson L, Kindbeiter K, Buffet T, et al.

Microenvironment-Driven Shift of Cohesion/Detachment Balance within Tumors Induces a Switch toward Metastasis in Neuroblastoma. Cancer Cell. 2017;32:427-443.e8.
11. Jarrosson L, Costechareyre C, Gallix F, Ciré S, Gay F, Imbaud O, et al. An avian embryo patient-derived xenograft model for preclinical studies of human breast cancers. iScience. 2021;24:103423.
12. Jarrosson L, Dalle S, Costechareyre C, Tang Y, Grimont M, Plaschka M, et al. An *in vivo* avian model of human melanoma to perform rapid and robust preclinical studies. EMBO Molecular Medicine. 2023;15:e16629
13. Scott DW, Gascoyne RD. The tumour microenvironment in B cell lymphomas. Nature Reviews Cancer. 2014;14:517–34.
14. Jaffredo T, Gautier R, Eichmann A, Dieterlen-Lièvre F. Intraaortic hemopoietic cells are derived from endothelial cells during ontogeny. Development. 1998;125:4575–83.
15. Denisenko E, Guo BB, Jones M, Hou R, de Kock L, Lassmann T, et al. Systematic assessment of tissue dissociation and storage biases in single-cell and single-nucleus RNA-seq workflows. Genome Biology. 2020;21:130.
16. van den Brink SC, Sage F, Vértesy Á, Spanjaard B, Peterson-Maduro J, Baron CS, et al. Single-cell sequencing reveals dissociation-induced gene expression in tissue subpopulations. Nature Methods. 2017;14:935–6.
17. Squair JW, Gautier M, Kathe C, Anderson MA, James ND, Hutson TH, et al. Confronting false discoveries in single-cell differential expression. Nature Communications. 2021;12:5692.
18. Nakagawa J, Takahata T, Hyodo R, Chen Y, Hasui K, Sasaki K, et al. Evaluation for pharmacokinetic exposure of cytotoxic anticancer drugs in elderly patients receiving (R-)CHOP therapy. Scientific Reports. 2021;11:785.
19. Huet S, Sujobert P, Salles G. From genetics to the clinic: a translational perspective on follicular lymphoma. Nature Reviews Cancer. 2018;18:224–39.
20. Delbridge ARD, Grabow S, Strasser A, Vaux DL. Thirty years of BCL-2: translating cell death discoveries into novel cancer therapies. Nature Review Cancer. 2016;16:99–109.
21. Blombery P, Lew TE, Dengler MA, Thompson ER, Lin VS, Chen X, et al. Clonal hematopoiesis, myeloid disorders and *BAX* -mutated myelopoiesis in patients receiving venetoclax for CLL. Blood. 2022;139:1198–207.
22. Dujon AM, Aktipis A, Alix-Panabières C, Amend SR, Boddy AM, Brown JS, et al. Identifying key questions in the ecology and evolution of cancer. Evolutionary Applications. 2021;14:877–92.

23. Zhang L, Nomie K, Zhang H, Bell T, Pham L, Kadri S, et al. B-Cell Lymphoma Patient-Derived Xenograft Models Enable Drug Discovery and Are a Platform for Personalized Therapy. Clinical Cancer Research. 2017;23:4212–23.
24. Di Gaetano N, Cittera E, Nota R, Vecchi A, Grieco V, Scanziani E, et al. Complement activation determines the therapeutic activity of rituximab in vivo. The Journal of Immunology. 2003;171:1581–7.
25. Zelenetz AD, Salles G, Mason KD, Casulo C, Le Gouill S, Sehn LH, et al. Venetoclax plus R- or G-CHOP in non-Hodgkin lymphoma: results from the CAVALLI phase 1b trial. Blood. 2019;133:1964–76.
26. Márquez-Jurado S, Díaz-Colunga J, das Neves RP, Martinez-Lorente A, Almazán F, Guantes R, et al. Mitochondrial levels determine variability in cell death by modulating apoptotic gene expression. Nature Communications. 2018;9:389.

Acknowledgements

The authors thank the Institut Carnot Calym for having provoked the scientific collaboration and provided access to the CeVi_Collection. The authors also thank the Centre de Ressources Biologiques CRB-Sud from Hospices Civils de Lyon, Lyon Sud hospital pharmacy department for having provided RCHOP compounds. We thank Yann Guillermin for his help in data collection. We thank Sabrina Baaklini, Pierre Milpied, Bertrand Nadel, Jerome Tamburini, and Bruno Tesson for helpful scientific discussions.

We acknowledge the contribution of SFR Biosciences (UAR3444/CNRS, US8/Inserm, ENS de Lyon, UCBL) lentivectors production facility (Gerland) and cytometry facility (Lyon Sud). We thank ChatGPT for English editing.